Development of Automatic Landing Flight Experiment (ALFLEX) Vehicle

Tetsuhiko UEDA[*1], Motoyuki INABA[*2], Masakazu SAGISAKA[*2], Kouhie TANAKA[*3], Eiji TANIKAWA[*3], Masakazu TAKAI[*3], Kazunobu UMEKI[*3], Junichi KIMURA[*3], Shigeru MACHIDA[*3]

ABSTRACT

An automatic landing technology is one of the key technologies necessary for the Japanese space shuttle "HOPE". The ALFLEX (Automatic Landing Flight Experiment) vehicle is an unmanned, 37% scaled model of HOPE, which is used to establish the fundamentals for fully automatic landing. The configuration of ALFLEX is simulating dynamically a HOPE baseline and its flight profile assumes only the landing phase. Conventional aluminum alloy forms the main structures of the vehicle with some FRP for the skin panels with double curvature. The vehicle is equipped with a completely independent electric system for the automatic landing and it has also an emergency system for ground safety. Ready made devices have been used to reduce the cost and the time needed for manufacture. The results of experiments confirmed that the automatic landing technology was suitable for use in the unmanned vehicle. Significant flight data, including the low-speed aerodynamic characteristics have been obtained using this sub-scale model.

1. Introduction

The key technologies necessary for the HOPE (H-II Orbiting Plane) include the fabrication of hot structures which can tolerate extremely high temperatures during re-entry into the atmosphere and the technology for a fully automatic landing system that enables a return of the unmanned vehicle from orbit to a 3,000-meter runway. The Automatic Landing Experiment (ALFLEX) has been performed to demonstrate one of these key technologies.

The ALFLEX vehicle is designed to land at a target runway automatically after its release from a helicopter at an altitude of 1,500m. It is preferable to use a similar vehicle to confirm the techniques in the landing phase of HOPE while we had several conditions that the runway should be less than 1,000m, that the dynamic similarity rule was

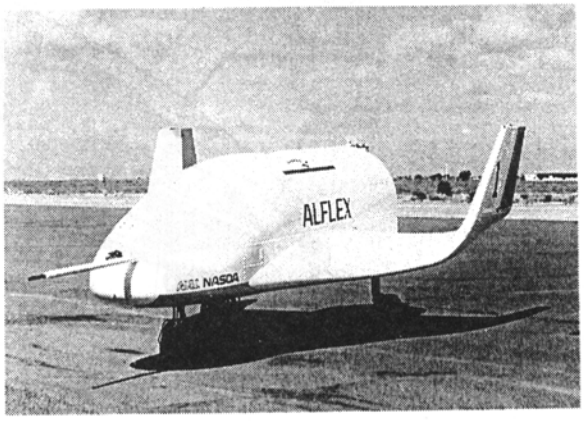

Fig. 1 ALFLEX Vehicle

*1 National Aerospace Laboratory
*2 National Space Development Agency of Japan
*3 Fuji Heavy Industry

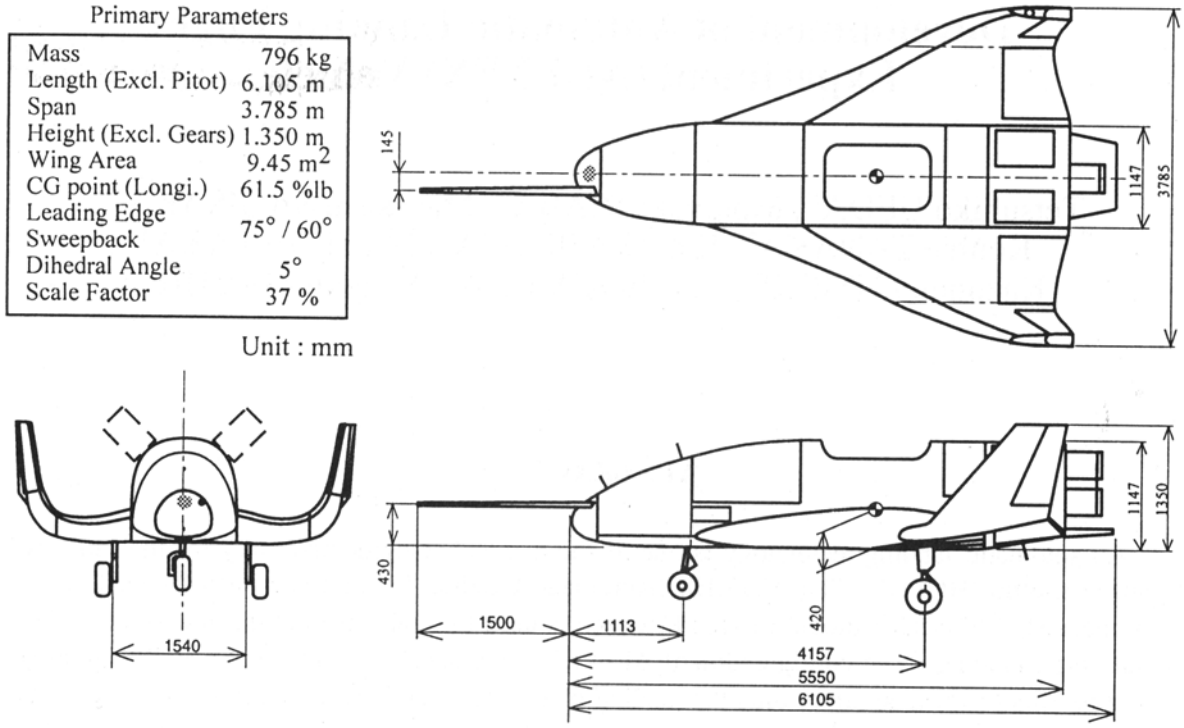

Fig. 2 Three Plan Views of Vehicle

required, that prefabricated equipment was used to save costs and time, and that the schedule was limited to a very short time for designing, manufacturing, and developing.

The design started in the spring of 1993 and the flight experiments ended successfully in the middle of 1996. This paper describes the development of ALFLEX vehicle and its experimental results.

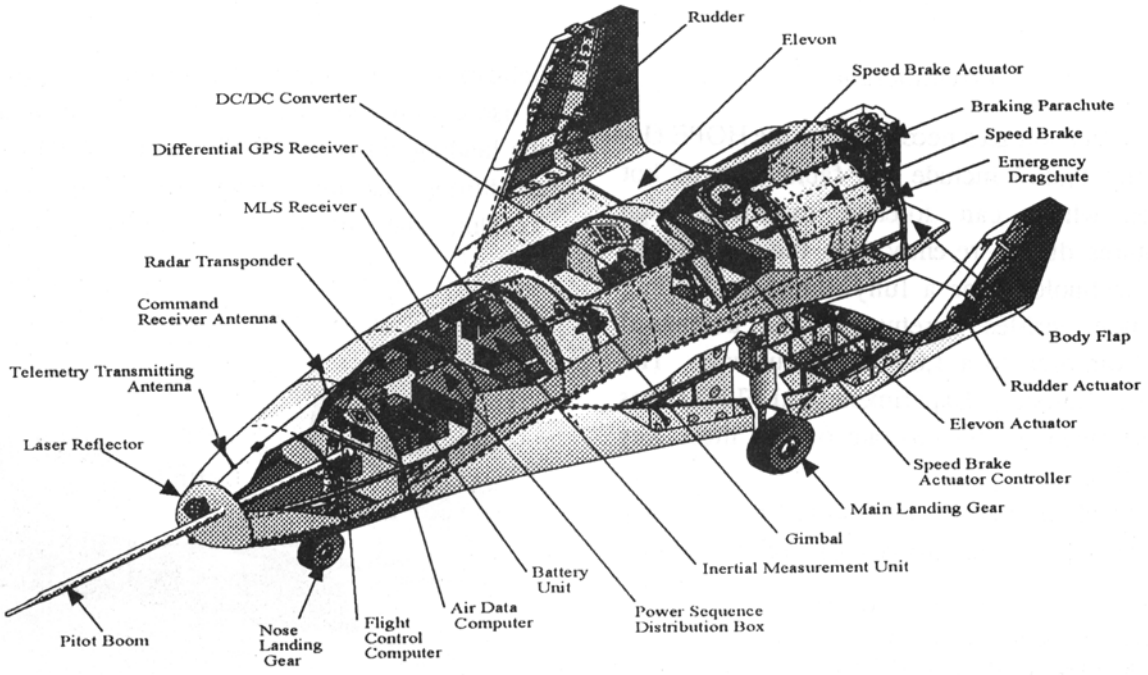

Fig. 3 Onboard Equipment

2. Outline of the Vehicle

A photograph of the ALFLEX vehicle and its three plan views are shown in Figs. 1 and 2, respectively. The vehicle is a 37% scaled model of a 20-ton-class HOPE baseline of 1992 and the aerodynamic contour simulates HOPE04C in terms of the basic aerodynamic characteristics. Apart from the baseline of HOPE, some features unique to this experimental vehicle are fixed landing gears, a nose boom for the air data system, and a relatively large cutout of the fuselage for a flight cable attached to the gimbals at the center of gravity. A braking parachute and an emergency dragchute are also equipped in the boxes located at the aft fuselage. The total mass after some improvements of the structure resulted in 796kg and a change of the center of gravity was 1mm forward in the x-direction(3412mm), 3mm left in the y-direction, and 21mm down in the z-direction(399mm) from the design.

The onboard equipment of the vehicle is shown in Fig. 3. The vehicle system consists of six subsystems: (1)the structural system containing the main wings and fuselage, (2)the actuator system containing the control surfaces of the elevons, rudders and speed-brakes, (3)the navigation, guidance and control system which estimates the position and speed, of guiding the vehicle to a prescribed flight path, and of controls the attitude of the vehicle, (4)the communication and measurement system which senses and transmits the onboard data, (5)the electric power/signal supply system which distributes signals and supplies power to the onboard instruments, and (6)the emergency system which makes the vehicle spin down within the limited area in case of coursing out from the prescribed flight path for purposes of ground safety. Every subsystem is a single system except for the emergency system which is dual.

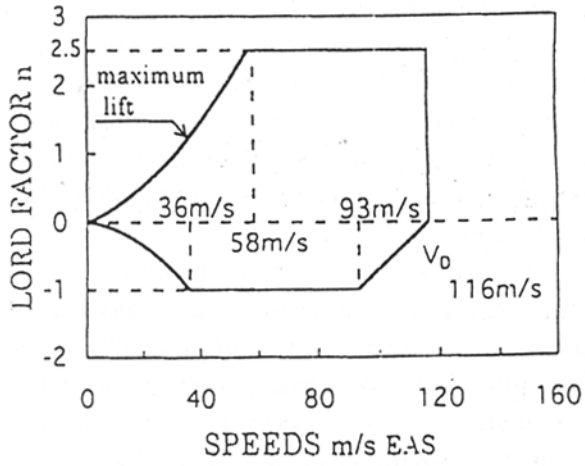

Fig. 4 Flight Envelope

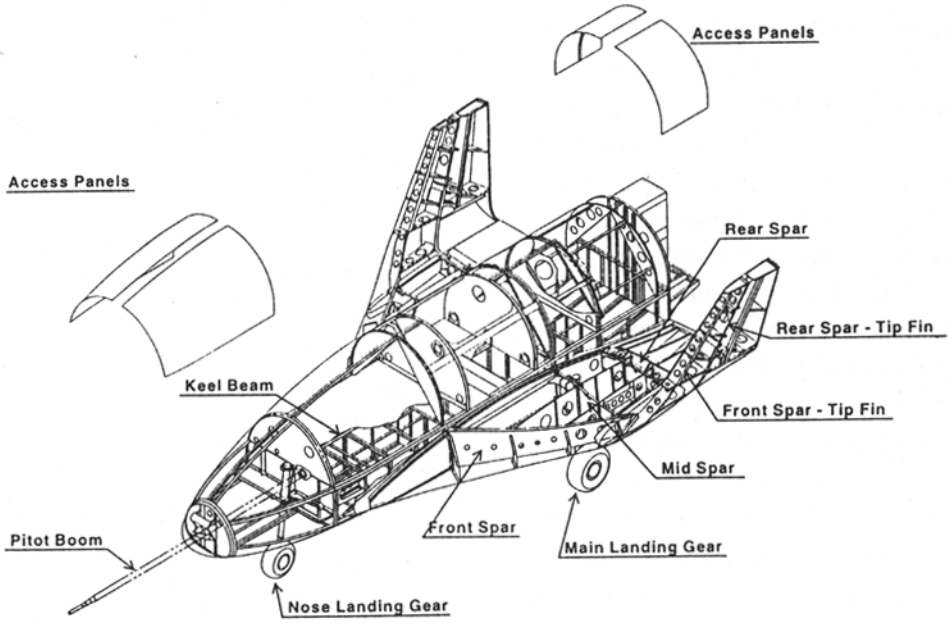

Fig. 5 Vehicle Structure

3. Development of the Vehicle

3.1 Structural system

3.1.1 Airframe

The structural design of ALFLEX follows the specifications of conventional aircraft even though it is unmanned. The safety factor was set at 1.5 to take into account the unknown circumstances of experimental landing phase; this was greater than the 1.25 which is typically used for unmanned vehicles. As a matter of course, the thermal protection system for aerodynamic heating was not included in the design concept.

The design flight envelope of maneuver load specified for the ALFLEX is shown in Fig. 4. The maximum load factor 2.5, which is the same as that of a transport airplane, is based on the assumption that there will be no extraordinary maneuvering during the experiments. An assumed cruising speed is V_C =93m/s (180kt) having sufficient margin and the maximum dive speed V_D=116m/s which is 25% higher than V_C.

The conventional aluminum alloy in riveting structures was used as the main material for the airframe to avoid developing a new type of structure. Only skin panels with double curvature are made of low temperature thermo-set GFRP because of saving costs and time. The vehicle can be disassembled into three parts to facilitate loading into the containers of a road truck.

The structure is depicted in Fig. 5. The main wings have three spars. Front and mid spars join together at the wing extremity to be connected to the front spar of a tip-fin. Intercostals at the joint were added later to increase stiffness against tip-fin vibrations. The main wing is connected to the carry-through under the instrument floor with four shear bolts at the mid and rear spars and with a pin at the front spar. The fuselage has a keel beam with four longerons, eight bulkheads, and one floor. The nose gear is located at the front edge of the keel. Most of the instruments are placed on the floor in front and aft instrument rooms. The 500kg hanging equipment loads on the two bulkheads and outer skins at "to and fro" of a gimbals' room. These structures are connected to the floor and longerons of the fuselage.

Figures 6 and 7 show the static tests and the ground vibration tests, respectively. The design strength was proven by applying 60% of the limit load at the tests. The calibrations of the strain sensors were also carried out in these tests.

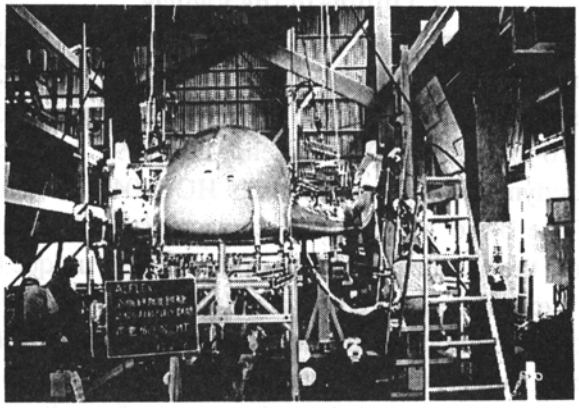

Fig. 6 Static Load Tests

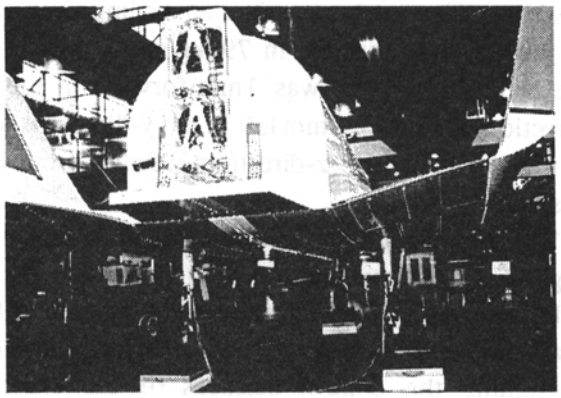

Fig. 7 Ground Vibration Tests

In the vibration tests, a laser Doppler vibration meter was used to detect vibration modes of the entire structure. The results of the tests showed that the natural frequency of the Pitot boom was raised from 5Hz to 15Hz by replacing by the CFRP pipe.

3.1.2 Landing gears

In the design of landing gears of ALFLEX, those of the domestic product aircraft, FA-200, satisfy the requirements so that three assemblies were utilized with one for landing gear tests. The tires were, however, replaced due to the high-speed touch down. Braking pressure is supplied by hydraulic accumulator and the braking system is equipped with an anti-skid braking system(ABS) assuming that the surface of the runway is unpaved. Tone

wheels are added to the original wheels for the ABS. Landing gears were tested on the brake-tester drum to check the design performance of braking and steering as can be seen in Fig. 8.

3.1.3 Braking parachute

In order to reduce the stopping distance, the ALFLEX has a braking parachute. A pilot chute which first extracts the main chute is ejected upward, in accordance with the results of the wind tunnel tests. Every chute door is operated by an independent solenoid. The dragchute of the emergency system is almost the same as the braking parachute except for an offset at the attachment in order to make the vehicle fly unbalanced when the chute is open.

3.1.4 Gimbals

The vehicle furnished with gimbals allowing ± 30deg allowance at the center of gravity to enable a five-degree-of-freedom flight by one constraint cable. The keel beam has a hollow at the location of the gimbals. Each gimbal-frame has a potentiometer to measure the gimbal -angles.

3.2 Actuator system

The actuator system includes elevon actuators, rudder actuators, and speed brake actuators. Each control surface is driven and controlled by each independent actuator and controller. The flight controllability requirements made it necessary to design high-performance electromagnetic rotary actuators for this vehicle using the latest technology. Every control surface is linked with the actuator by rods using typical aircraft linkage, which makes the link both tight and adjustable. The block diagram and the performance of the actuator system are shown in Fig. 9 and in Table 1, respectively.

The functions of actuators were checked by

Table 1 Performance of Actuator System

Performance Requirement	Rudder	Elevon	Speed Brake
Max Hinge Moment Nm	2.0×10^2	3.9×10^2	1.2×10^3
Max Angular Velocity deg/s (No Load)	150	80	30
Frequency Response Hz (45deg phase delay)	6	6	2
Output Operating Range deg	-35~+35	-35~+25	0~60
Output Characteristics	**Rudder**	**Elevon**	**Speed Brake**
Max Hinge Moment Nm	2.8×10^2	4.0×10^2	1.2×10^3
Max Angular Velocity deg/s (No Load)	240	156	30
Frequency Response Hz (45deg phase delay)	6	6	2
Output Operating Range deg	-35~+35	-35~+25	0~60

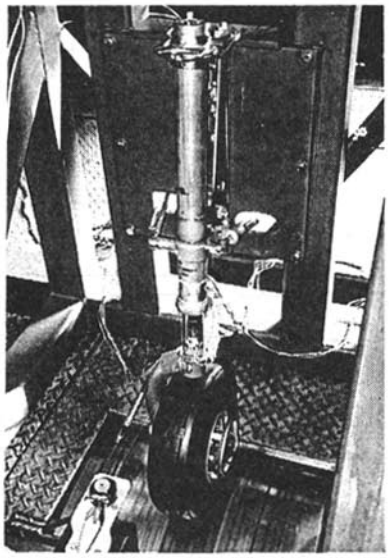

Fig. 8 Landing Gear Tests

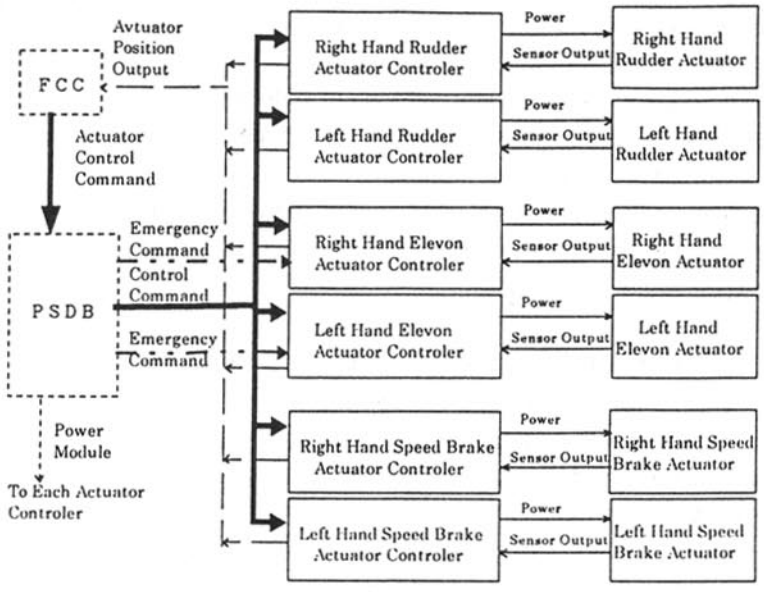

Fig. 9 Block Diagram of Actuator System

various development tests to ensure that they meet the requirements. A thermal environment test, a vibration test, an EMI test and a duration test were carried out for each actuator. These tests confirmed the functions of the elevons, rudders, and speed brakes. As for the EMC test, a part of the requirement was not satisfied in the radiative interruption. This could be resolved, however, by the arrangement of the system because the violated level was not so large.

In the domestic hanging tests, potentio-meters were additionally attached to each control surface to obtain the mechanical performance of the control system by measuring the angles of deflections directly during excitation of the surfaces. Figure 10

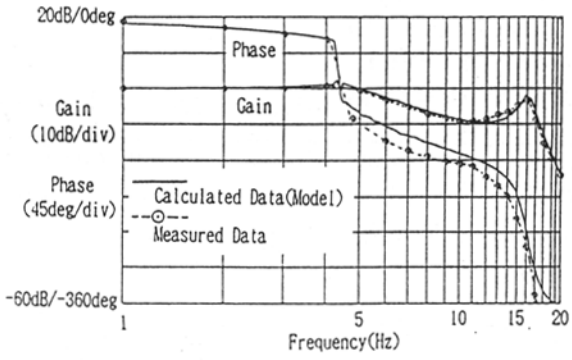

Fig. 10 Frequency Response of Elevon Actuator (Input: ±5deg; Non-Linear region)

shows a typical elevon response in the nonlinear region involving some effects of limiters. A corresponding simulation result with the mathematical model is also shown in the figure. As can be seen, the excellent agreement between these results is more than enough to evaluate the performance and the comprehensive actuator math-model, which could be used as a reliable tool for confirming the controllability before the experiments in Australia.

3.3 Communication and measurement system

The communication and measurement system has a function of acquiring the data measured and monitored by the power sequence distribution box (PSDB), the flight control computer (FCC), and the various sensors. It transmits these data via VHF telemetry as well as recording the data on the onboard recorder in accordance with a command from the FCC. The system also includes a radar transponder providing the radar tracker on the ground with signals for the tracking flight path. A block diagram of the communication and measurement system is shown in Fig. 11.

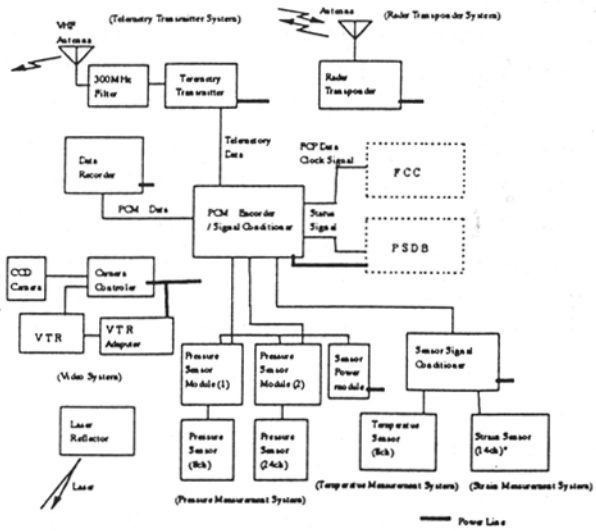

Fig. 11 Block Diagram of Communication & Measuremeent System

As the development tests, antenna pattern tests were carried out for the VHF telemetry, the X-band transponder, the MLSR antenna, and the GPSR antenna. The laser reflector had been tested in advance at the Sendai Airport by using the onboard reflector itself installed in an experimental airplane.

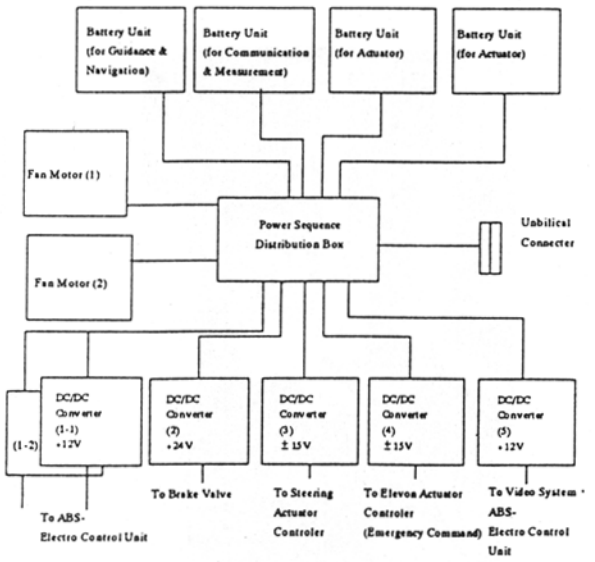

Fig. 12 Block Diagram of Electrical Power/ Signal Supply System

3.4 Electric power/signal supply system

Main components of the electric power/signal supply system are the battery units and the power sequence distribution box (PSDB) which can supply electric power to each instrument, distribute the discrete signals from FCC to corresponding devices, detect the release and the touch down, and have electric interfaces with the other AGE's and the mother helicopter. A block diagram of the electric power/signal supply system and the performances of the battery units and the PSDB are shown in Fig. 12, Tables 2 and 3, respectively.

table 2. Performance of Battery Unit

Type	Lead Storage Battery
Rated Voltage	28Vdc (14Vdc x 2)
Rated Capacity	31A/20minutes or more
Life Cycle	3times or more
Short Time Capacity	150A, 15 seconds
Storage Limited	2.5year(dry)

table 3. Performance of Power Sequence Distribution Box

Power Interruption	15msec
Chattering	Miss-Open should not be Exceeded neither 100×10^{-6}sec and 200pps
Output Signal	Voltage of Power Supply Bus, Inhibit of Launch, Inhibit of Shoot, Launch monitor, Parachute monitor, Brake monitor, Landing monitor, Power Source monitor, Status of Relay-contact monitor, Actuator Command monitor, etc.
Input Signal	Landing monitor, Actuator command, Brake command, Parachute command, Inhibit of Launch/shoot command, Power Source command, Data Recording command, etc.

Specifications for the electromagnetic compatibility was based on MIL-STD-461A with some relaxation to accommodate prefabricated instruments. An analysis of electric power consumption was carried out to evaluate the allowances in voltage and current. In the worst case, the voltage supply for a command receiver becomes 22.8V, violating the lower limit of 24V. For this device, an evaluation test was performed down to 22V and the nominal capability at 22.8V was confirmed. The lead storage battery, already developed for aircraft, is utilized to supply electric power of 28VDC for the vehicle. Four units with each having two batteries can supply subsystems separately, one for the guidance, navigation and control system, one for the communication and measurement system and the remaining two for the actuator systems.

The battery units underwent a capacity test and a duration test. For the capacity test, four units of the batteries were discharged as simulating a profile of power consumption of each bus, and we obtained the characteristics at the operational condition. The presumed functions were satisfied including the maximum current condition of 150A. For the duration test, the duration capability was confirmed by repeating the closed loop tests using battery power. The results showed a satisfactory duration time even for the hanging flights which lasted about 30minutes.

3.5 Emergency System

The purpose of this system is to spin down the vehicle when receiving an emergency command from the ground to restrict its scattering area for purposes of ground safety. The system consists of the emergency command receivers and an emergency dragchute. It is also linked to the flight safety components in other devices, such as the emergency circuit in PSDB, batteries, control

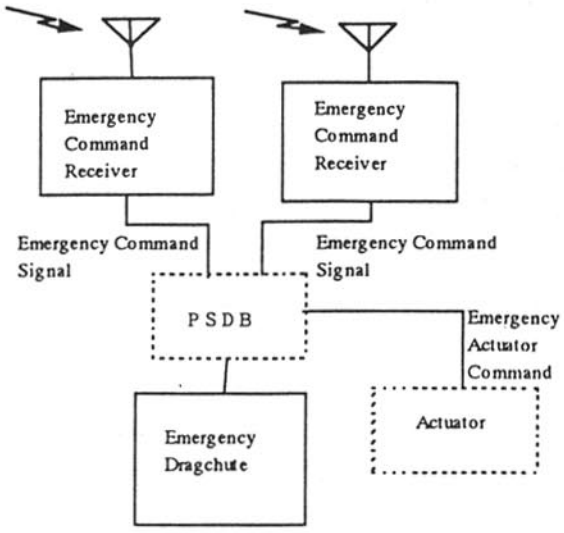

Fig. 13 Block Diagram of Emergency System

surfaces and so on. A block diagram of the system is shown in Fig. 13.

3.6 Ground roll tests (Domestic tests)

Figure 14 shows a ground roll test conducted at

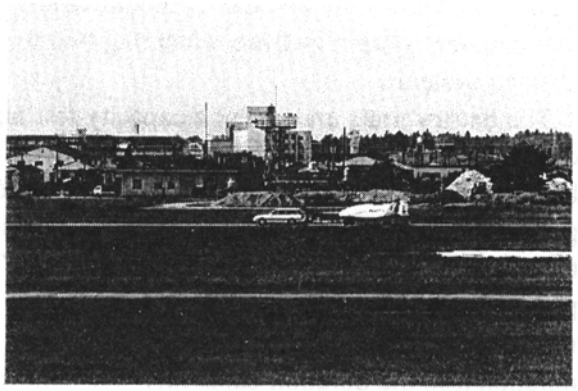

Fig. 14 Ground Roll Tests at Utsunomia

Utsunomia. In these tests, functions and capabilities of the devices relating with the ground roll were tested in actual runs:

(i) braking force satisfied its specifications at a speed of 50km/h:

(ii) deployment of a braking parachute was confirmed during the run at 70km/h with the speed brakes in a 40deg upright position:

(iii)alignment of the landing gears was adjusted to go straight in the neutral position: and

(iv)controllability of steering and braking with the FCC was confirmed at a speed of 15km/h.

3.7 Ground roll confirmation tests (Tests in Australia)

Tests similar to those mentioned above were performed after re-assembling the vehicle in Australia with the followings results:

(i) the radius of curvature in the straight run by keeping the nose wheel in a neutral position was more than the specification value of 200m:

(ii) functions of the IMU-MLS hybrid navigation and the guidance and control during the ground roll were confirmed at the 90km/h run: and

(iii) the ability of braking with the ABS was confirmed up to 90km/h and the braking pressure was properly adjusted.

4. Results of the Flight Experiments

4.1 Structural system

4.1.1 Flight load

The local maximum loads in each flight phase are plotted in Fig. 15 for all flights. In a typical flight,

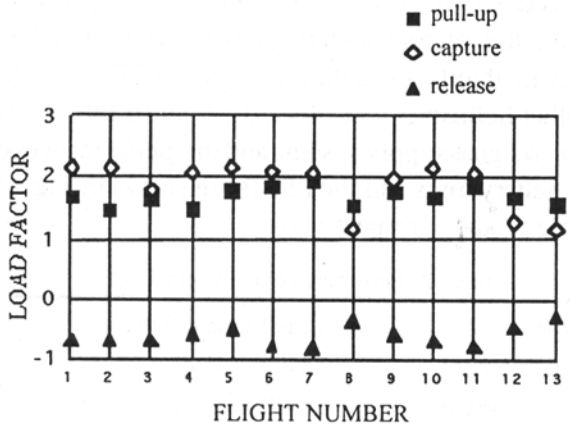

Fig. 15 Load at Free Flights

a negative load occurred first just after the release to accelerate downward, then a large positive load came to capture the nominal path and finally again a positive load entered at pulling up in the pre-flare phase before he runway threshold. The design load at pre-flare was a constant of 1.5. As can be seen, the results show relatively similar maximum loads at the pull-up in every flight and their average value was 1.7. The load at the capturing flight path depends on the release condition. The values less than those of the pull-up appeared in flights #08, # 12 and #13, all of which were the cases of off-set release. The negative loads at the release were also small in the absolute values in these cases. Negative loads after the release are not expected in the HOPE flight profile since these were due to the method of the present experiments. All loads were within the design envelope of maneuver from -1 to 2.5 (Fig. 4). The results validated the adequacy of the design setting.

4.1.2 Bending moment of the wings

Typical results of the output of strain gages at the wing roots are shown in Fig. 16 as the bending moment versus the vertical acceleration of flight # 10. As can be seen, the bending moments have a clearly linear correlation with the vertical acceleration of the flight. Some scattering around 1G equilibrium flight may be attributed structural

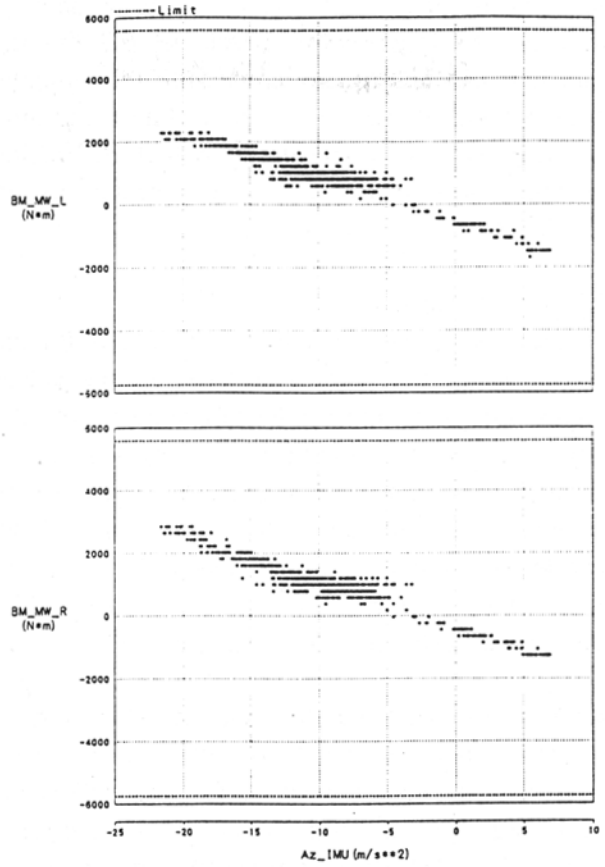

Fig. 16 Results of Bending Moment in Flight #10

vibration. The dotted lines in these figures correspond to the design limit which is sufficient for real flight data.

4.1.3 Structural vibrations

During the hanging tests, a vibration of about 27Hz was observed on the pitch rate measured by the IMU. Because this vibration depended upon the dynamic pressure, it might adversely affect the fight control if the dynamic pressure became large in free flights. The cause of the vibration was not clear. The large hole on the fuselage was suspected to make aerodynamic excitation on the bulkhead behind the IMU. Therefore, in Woomera, 20mm thick rubber foam for heat insulation was attached to the wall to attenuate the aerodynamic excitation and to increase the structural damping of the wall. This treatment decreased the vibration level by more than half. The vibration level in an actual free flight can be seen in Fig. 17 which shows a time history of the vertical acceleration at the first flight. The corresponding vibration can be seen in the interval from 20s to 40s of the history. The amplitudes were

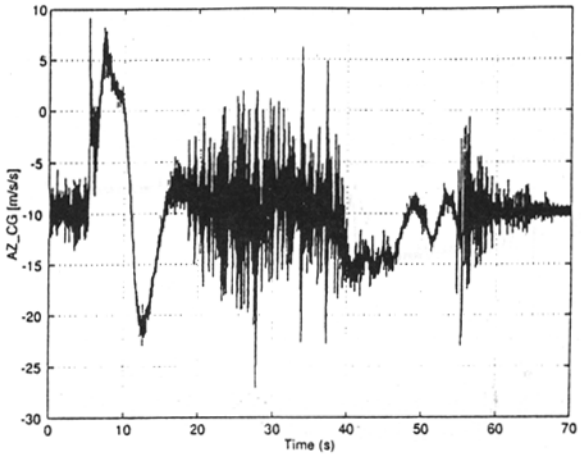

Fig. 17 Time History of Vertical Acceleration (#01)

less than $1G_{0\text{-}p}$ of the specification value except for several peaks due to shocks. This vibration was never anticipated during vehicle design. The vibration level after touch down which can be seen after the spikes at 56s and 57s which correspond to the shocks from the nose and main landing gears, respectively. The amplitudes were well below the design specification values. The time histories of the vertical acceleration of the other twelve flights were more or less at the same level.

4.1.4 Braking force

The braking pressure in an accumulator was initially adjusted to 4.1MPa based on the results of the ground roll tests. The test in Woomera from 70km/h resulted in activation of the ABS at a pressure of 6.1MPa, which led to an estimation of the friction coefficient as 0.7 at the dry runway surface.

The braking force was measured with the strain gages attached to the columns of the main landing gears. At the first flight, the barking force showed 30% difference between the left and the right brakes due to rough fitting of the disc and the linings. Considering the fact that the stopping distance of the first two flights was sufficiently short, the brake pressure was reduced to 2.1MPa to minimize the unbalancing force during braking. The time history of the braking force at flight #11 (Fig.18) showed no large differences any longer after braking of ten previous flights.

In order to evaluate the braking capability, the

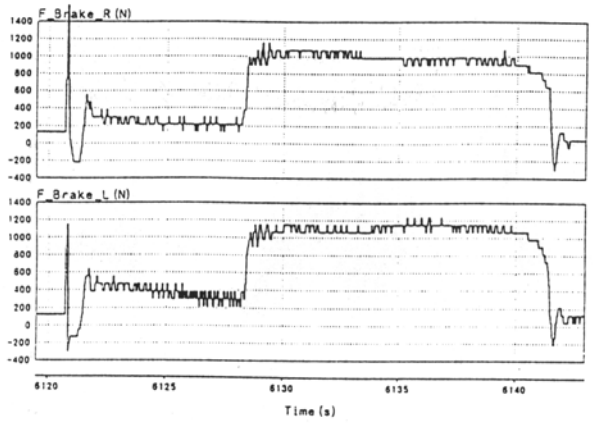

Fig. 18 Time History of Braking Force After Touch Down (#11)

stopping distances from touch down to the stop point for all flights are shown in Fig.19. Further, the kinetic energies of the vehicle at touch down are shown in Fig. 20. The braking parachute was not

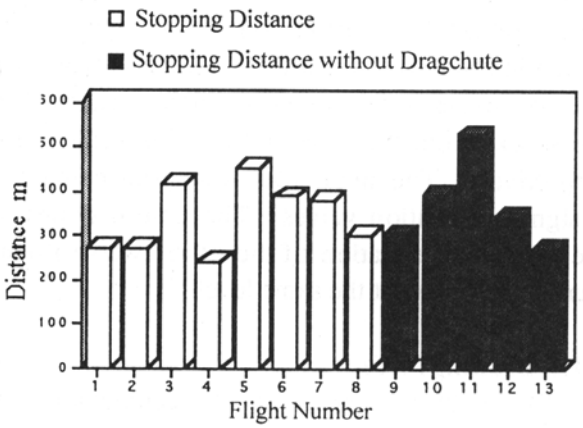

Fig. 19 Stopping Distance (From Touch Down Point to Stop Point)

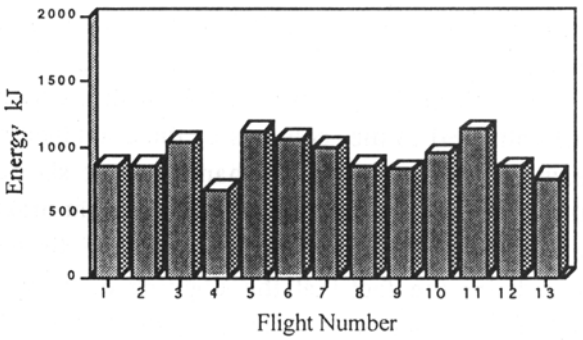

Fig. 20 Kinetic Energy at Touch Down

used after flight #09. As can be seen in these figures, the stopping distance depended obviously upon the kinetic energy, revealing that the fluctuations in the braking forces, including the aerodynamic drag due to winds, at these landings were not so large. The effects of the braking parachute can be seen by comparing the stopping distances with those starting from almost the same kinetic energy. These results show that the braking capability was satisfactory to stop vehicle on an 1,000m runway.

4.2 Actuator system

There were no apparent mal-functions on the movement of the control surfaces in the actual flights. Only the rudder deflection angles showed a difference from the command (0.6deg), which may be attributed to deformation at the attachment of the monitoring sensor due to the aerodynamic load. The temperature rise, which had been a concern before the experiments, was at most about 40℃ whereas the design limit allowed up to 80℃.

4.3 Communication and measurement system

There were no problems with the command receiver or the electric wave links of the telemetry, the emergency command, the radar link, the radio altimeter, the MLSR, or the DGPSR in any of the experiments. The other instruments also functioned satisfactorily in the experiments.

4.4 Electric power/signal supply system

We did not experience any trouble with this system throughout the experiments. The battery supplied sufficient power for the vehicle and functioned well in the charging rotations.

4.5 Emergency system

This system has never been operated during an actual flight and has not caused any serious interference with the other systems.

5. Conclusion

All 13 automatic landings were successful and were an important milestone in the development of HOPE. The data acquired in the experiments will be incorporated into the design of HOPE-X. The success of the first unmanned vehicle attempts in our country would not have been possible without the cooperation among the relating organizations including the Australian government.

ALFLEX Guidance, Navigation and Control

Yoshikazu MIYAZAWA[*1], Kazutoshi ISHIKAWA[*1],
Tatsushi IZUMI[*2], Masakazu SAGISAKA[*2],
Shigeru ASAI[*3], Takashi HATA[*3], Masahiro OHNO[*3] and Akihiro NISHIMURA[*3]

ABSTRACT

This paper introduces the Guidance, Navigation and Control System developed for the Automatic Landing Flight Experiment, ALFLEX. The system was developed to demonstrate technology readiness for the re-entry space vehicle's automatic landing. Lessons learned in the development are also discussed.

Key Words: HOPE, ALFLEX, Automatic landing, Flight test, Navigation, Guidance and Control

1. Introduction

A guidance, navigation and control (GNC) system was developed for the ALFLEX vehicle to land safely on a 1000-m runway. The vehicle is a 37% subscale model of a conceptual vehicle in the Japanese ongoing H-II orbiting plane (HOPE) program, where the model was one of the candidates in the 1992 conceptual design. In order to achieve the goal of the experiment while minimizing the cost and time for development, the ALFLEX program included the following principles for the GNC system design.

(1) Scaled model experiment
The GNC system as well as the experiment was designed to be dynamically similar to HOPE for the flight experiment to be a demonstration of HOPE landing technology readiness. Concerning wind and gust disturbance conditions, they also follow the rule of similarity. The wind and gust disturbance conditions were defined so that the HOPE can land safely against those of US military specifications, which are widely used.

[*1]National Aerospace Laboratory, Tokyo, Japan
[*2]National Space Development Agency of Japan, Tokyo, Japan
[*3]Mitsubishi Heavy Industries Co. Ltd., Nagoya Aerospace Systems, Nagoya, Japan

(2) Off-the-shelf hardware
In order to reduce the cost and time of development, the GNC system uses prefabricated hardware, and it is designed based on the performances of these components. The only exception is differential GPS, i.e. navigation uses the components under the non-critical conditions for the experiment safety.

(3) No redundant GNC system
Although the HOPE vehicle will have a highly reliable redundant system, the ALFLEX vehicle has a non-redundant system of single channel components. The choice of this structure satisfies the experiment objective and is reasonable based on the limited number of experiments, the non-hazardous nature of the experiment area, and the fact that each component has high reliability, comparable to general components in commercial use.

(4) Limited development tests
The design employs data of the minimum essential tests, such as wind tunnel tests and simple ground tests, otherwise it uses catalogue performance data of components. The GNC system design is robust enough to tolerate these errors obtained in limited tests. The ALFLEX perform a special preliminary flight test, called the "5 degrees of freedom" hanging flight test in order to reduce the risk of the first flight, but the data is not prerequisite for the GNC design.